Lithospheric anisotropy beneath the Pyrenees from shear wave splitting

Guilhem Barruol, Annie Souriau, Alain Vauchez, Jordi Diaz, Josep Gallart, José Tubia, Julia Cuevas

JOURNAL OF GEOPHYSICAL RESEARCH, VOL 103, NO B12, PAGES 30039-30053, DECEMBER 10, 1998

Lithospheric anisotropy beneath the Pyrenees from shear wave splitting

Guilhem Barruol,[1] Annie Souriau,[2] Alain Vauchez,[1] Jordi Diaz,[3] Josep Gallart,[3] José Tubia,[4] and Julia Cuevas[4]

Abstract. We investigate upper mantle anisotropy beneath the Pyrenean range along three N-S profiles across the mountain belt. The results of a first profile that operated in 1993 in the central part of the belt have been presented elsewhere. We present the results of two other profiles that ran in 1995-1996 and 1996-1997 in the eastern and western part of the belt, respectively and propose an interpretation of the whole results. Teleseismic shear waves (*SKS*, *SKKS*, and *PKS*) are used to determine splitting parameters: the fast polarization direction ϕ and the delay time δt. Teleseismic shear wave splitting in the eastern Pyrenees displays homogeneous ϕ values trending N100°E and δt values in the range 1.1 to 1.5 s. A station located in the southern Massif Central, 100 km north of the range, is characterized by different splitting parameters (ϕ = N70°E, δt = 0.7 s). In the western part of the belt, anisotropy parameters are similar across the whole belt (ϕ = N110°E and δt = 1.3 to 1.5 s). Most of the measured delay times, including those obtained in the central part of the range, are above the global average of the *SKS* splitting (around 1 s). At the belt scale, ϕ is generally poorly correlated with recent estimations of the absolute plate motion, which predicts a fast direction ranging between N50°E and N80°E. Instead, the orientation of ϕ (N100°E) is parallel to the trend of the Pyrenean belt but also to Hercynian preexisting structures. This parallelism supports an anisotropy primarily related to frozen or active lithospheric structures. We show that a signature related to the Pyrenean orogeny is likely for the stations located in the internal domains of the belt. By contrast, the anisotropy measured at the stations located on the external parts of the belt could reflect a pre-Pyrenean (Hercynian) deformation. We suggest that a late Hercynian strike-slip deformation is responsible for this frozen upper mantle anisotropy and that the Pyrenean tectonic fabric developped parallel to this preexisting fabric. Finally, no particularly strong splitting is related to the North Pyrenean Fault, commonly believed to represent the plate boundary between Iberia and Eurasia.

1. Introduction

Although rock physics indicates that lithospheric behavior is primarily controlled by its upper mantle constituent, our knowledge of plate tectonics mainly derives from surface geology and crustal structures inferred from geophysical data. This last decade, however, shear wave splitting has been used as a mean to fill this gap. From indirect investigation of pervasive upper mantle structures [see *Silver*, 1996, and references herein], seismic anisotropy has become a new tectonic tool to characterize upper mantle flow. Seismic anisotropy at great depth is indeed broadly accepted to result from intrinsic elastic anisotropy of rock-forming minerals and from their preferred orientations developed in response to tectonic flow. Olivine, which represents the main upper mantle constituent and which is the most anisotropic peridotite phase, controls upper mantle anisotropy [Nicolas and Christensen, 1987]. Since shear wave splitting is a direct result of anisotropy, and hence rock deformation, it is possible to investigate deep structure in relation to plate tectonics, in particular, beneath plate boundaries and mountain belts, where strong upper mantle deformations are expected to occur.

The Pyrenees result from an Albian-Cenomanian strike-slip motion of Iberia relative to Eurasia, followed by an Eocene collision between the two plates [e.g., Choukroune, 1992; Olivet, 1996]. The belt, oriented roughly E-W, exhibits a nearly cylindrical symmetry with several units (Figure 1): the Pyrenean Axial Zone is made of Paleozoic rocks and displays pervasive structures formed during the Hercynian orogeny. It is bounded northward by the North Pyrenean Fault (NPF), thought to represent the plate boundary in pre-Albian times. North of this fault, the North Pyrenean Zone (NPZ) is primarily composed of deformed Mesozoic rocks, which incorporate small Hercynian massifs and lherzolite bodies. The North Pyrenean Zone overthrusts the Aquitaine basin to the north. The NPZ structure is the consequence of the opening of the bay of Biscay and the related rotation of Iberia with respect to Eurasia 100 Myr ago: These events created a rift zone at the present location of the North Pyrenean Zone [e.g., Choukroune, 1992], which favored high-temperature and low-pressure metamorphism [Golberg and Leyreloup, 1990] and lherzolite emplacement [Vielzeuf and

[1]Laboratoire de Tectonophysique, CNRS, Université Montpellier II, Montpellier, France.
[2]Laboratoire de Dynamique Terrestre et Planétaire, CNRS, 14 av Belin, 31055 Toulouse, France.
[3]Institut de Ciències de la Terra, CSIC, Barcelona, Spain.
[4]Departamento de Geodinamica, Universidad del Pais Vasco, Bilbao, Spain.

Paper number 98JB02790.
0148-0227/98/98JB-02790$09.00

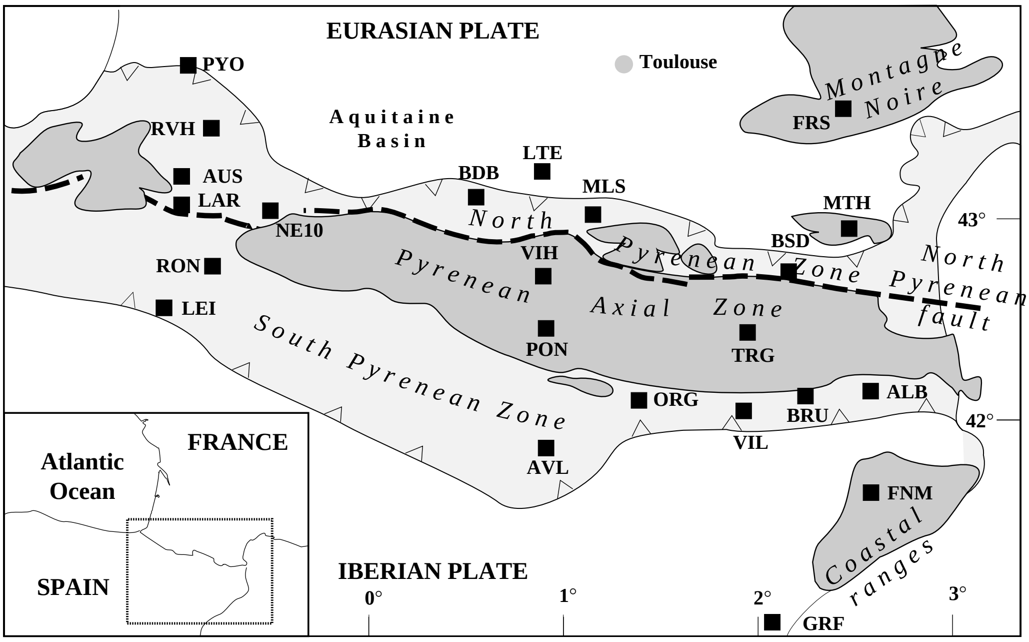

Figure 1. General map of the Pyrenees showing the tectonic units and the station locations.

Kornprobst, 1984]. South of the Paleozoic Axial Zone, the South Pyrenean Zone is made of Mesozoic and Cenozoic sedimentary nappes overthrusting the Ebro basin to the south.

Since teleseismic shear wave splitting is a marker of upper mantle tectonic fabric, our aim is to give some insights into the deep structures of the Pyrenees and to investigate the influence on seismic anisotropy of the various tectonic episodes that occurred in the Pyrenees. We focus our discussion on the upper mantle accommodation of the relative strike-slip motion and collision between the plates, on the signature of the North Pyrenean Fault and also on the departure of the belt from cylindrical symmetry. The role of present-day tectonics and the influence of preexisting structures is also discussed.

2. Data and Results

Teleseismic events were recorded during three experiments along N-S profiles (see station location Figure 1): the first experiment described by *Barruol and Souriau* [1995] ran in 1993 in the central part of the belt; the second experiment ran in 1995-1996 across the eastern Pyrenees, and the third one ran in 1996-1997 in the western part of the belt.

For the eastern experiment, eight broadband three components seismic stations from the French LITHOSCOPE network were installed between the southern Massif Central (France) and Barcelona (Spain). Four additional stations from the Institute of Earth Sciences from Barcelona were installed for a few months on the Spanish side of the belt, either at sites later occupied by LITHOSCOPE stations (ORG and ALB) or at sites in the Catalan coastal ranges (BRU and FNM). These stations provide anisotropy measurements laterally off the N-S profile (see Table 1 for the station location). The experiment ran between January 1995 and April 1996. Continuous recording at 15 samples per second with Lennartz 5 s sensors allowed us to select and extract teleseismic events of convenient distances and magnitudes suitable for *SKS*, *SKKS* and *PKS* splitting measurements. From the whole data set of teleseismic events located at a distance greater than 85° and magnitude greater than 5.8, about 40 events were kept after visual inspection (Table 2). In order to avoid noise contamination of the splitting measurements, only events characterized by signal to noise ratio of the *SKS* phase higher than 2 were kept.

For the western profile, six broadband or intermediate period, three-component stations from the LITHOSCOPE network and from the Pyrenean seismic survey network were installed during the period July 1996 to May 1997. Unfortunately, these stations did not record continuously, and due to small data storage capacity, a rather high threshold in record triggering was used. Moreover, the proximity of the Atlantic Ocean induces a high level of microseismic noise. This explains the smaller number of events obtained during this experiment.

The splitting of seismic shear waves is a direct effect of seismic anisotropy: If one excepts the case where the incidence plane is coincident with one of the polarization plane, a polarized shear wave crossing an anisotropic medium is split into two perpendicularly polarized waves that propagate at different velocities. Anisotropy parameters may be retrieved from three-component seismic records: the difference in arrival time (δt) between the two split waves, which depends on the thickness and intrinsic anisotropy of the anisotropic medium, and the orientation of the split waves polarization planes (ϕ for the fast wave), which are related to the orientation of the structure. The shear wave splitting measurements were obtained using the *Silver and Chan* [1991] algorithm. This method assumes a hexagonal symmetry of anisotropy with a horizontal symmetry axis and determines the anisotropy parameters, $\phi$and δt, that best removes energy on the transverse component of the seismogram for a selected time window. Some examples of splitting measurements are shown Figure 2. Despite the small number of measurements performed in western Pyrenees, event 97023 recorded at AUS and LEI provides an example of a well constrained result. Event 95291 in eastern Pyrenees (TRG) and southern Massif Central (FRS) gives a less constrained measurement but clearly shows a different signature between the two areas.

The event origins and locations (Table 2) are taken from the

Table 1. Station Locations, Mean Splitting Parameters with 1σ errors

Station	Latitude, °N	Longitude, °E	Elevation, m	φ, deg	σφ, deg	δ*t*, s	σ δ*t*, s	Number of Measurements
FRS	43.365	2.447	860	75	4	0.70	0.10	6
MTH	42.939	2.534	620	102	2	1.29	0.09	11
BSD	42.795	2.156	1110	97	4	1.12	0.11	10
TRG	42.502	1.967	1520	99	3	1.45	0.09	15
ALB	42.314	2.721	120	101	6	1.80	0.21	6
ORG	42.227	1.332	998	101	4	0.98	0.16	3
VIL	42.136	1.891	795	89	3	1.07	0.08	19
GRF	41.152	1.891	280	86	2	1.75	0.11	14
FNM	41.762	2.433	222	120	5	1.25	0.18	1
BRU	42.283	2.186	223	96	5	0.93	0.01	3
PYO	43.538	-0.880	180	112	5	1.45	0.28	1
RVH	43.348	-0.847	160	110	2	1.45	0.23	1
AUS	43.152	-0.933	210	110	5	1.25	0.03	3
LAR	43.023	-0.938	540	116	3	1.39	0.13	3
RON	42.797	-0.964	470	102	4	1.45	0.12	2
LEI	42.652	-1.220	250	105	4	1.48	0.14	2

U.S. Geological Survey (USGS) Preliminary Determination of Epicenters, and the phase arrivals were computed using the IASP91 Earth reference model [*Kennett*, 1995]. Most individual measurements were performed on earthquakes occurring at distances in the range 85 to 115°. The *SKS* phase was generally used, but for some events, the whole *SKS* + *SKKS* wave train was selected. For some events occurring at distances between 130 and 140°, *PKS* and *SKKS* phases gave good results (event 95226, for instance). Many events do not show any evidence of signal on the transverse component. Such events, are classically considered as "null" results and indicate either that there is no anisotropy beneath the station or that the initial polarization direction of the *SKS* wave is parallel to the fast or slow direction in the anisotropic layer. This second possibility is the only considered when non-null measurements are obtained at the same station. These null results are also shown in Figure 3, on the right. Table 3 summarizes the individual splitting parameters. For each, we report the split phase on which the measurement has been performed, the distance and backazimuth of the event, and the splitting parameters (φ, δ*t*) with their 1σ uncertainty, determined from the 95% confidence interval in the (φ-δ*t*) domain. We also ascribe a quality factor (good, fair, or poor) to the measurements depending on the signal to noise ratio of the initial phase, the rectilinear polarization of the particle motion in the horizontal plane after anisotropy correction, and the wave form correlation between the fast and slow split shear waves. This evaluation of the quality is particularly useful in temporary experiments, when relatively few data are available. Few individual measurements were performed on earthquakes occurring at distances less than 85°. Event 95231, occurring at a distance of about 78° is one of the exceptions: at this distance, and given the depth of this event (125 km), the *sSKS* phase arrives after the *S, ScS,* and *sS* phases. Splitting measurements on such *sSKS* phases have been done with confidence because the S and ScS phases were impulsive and did not appear to contaminate the following s*SKS* phase. A second exception is event 97084, at a distance of 82°. Since this event is very deep (609 km), we assumed that the splitting occurs primarily beneath the station and not at the source and used the direct *S* wave to characterize the anisotropy.

A strikingly large difference in the number of splitting measurements appears between the eastern and the western stations (Figure 3). This is mainly related to two factors: the eastern experiment ran for a much longer time (16 months as compared to 10 months in the western Pyrenees) and also continuous recording strongly increased the number of available data. It appears from Figure 3 and Table 3 that good measurements at a given site may display some variations in splitting parameters (10 to 20° in azimuth and 0.1 to 0.2 s in delay time); this may result from lateral heterogeneities, but this may also indicate that the initial assumptions used for calculations are not fulfilled, that is, that several layers of anisotropy exist beneath the station and/or that the anisotropy symmetry axis is dipping. Such structures should result in an apparent variation of the splitting parameters correlated with the event backazimuth, with a periodicity of π/2 and π, respectively [*Savage and Silver*, 1993; *Silver and Savage*, 1994]. No such systematic variation is clearly detected, but the amount of data obtained during the temporary experiments is too small to allow a confident characterization of such properties. In most cases, however (if we except FRS, see discussion below), 95% confidence intervals overlap in the φ-δ*t* plot, and individual splitting measurements display a coherent pattern of nulls and non nulls, suggesting a model of anisotropy dominated by a single anisotropic layer.

We test the dependence of the splitting parameters on the signal frequency because it may give some insights on the degree of heterogeneity of the anisotropic layer and on the lateral or radial variations of the structures [*Marson-Pidgeon and Savage,* 1997]. On few constrained events (97023 at LEI and AUS and 95291 at TRG), we used the method from *Marson-Pidgeon and Savage* [1997] in which the splitting parameters are analyzed as a function of the dominant period of the split phase. We filtered the signal using narrow band-pass filters and determined the corresponding splitting parameters. By slightly moving the band-pass window in the frequency domain, we investigated possible variations in the φ-δ*t* parameters as a function of the dominant

Table 2. Events used for *SKS* splitting measurements

Event	Date	Time, UT	Latitude, °N	Longitude, °E	Depth, km	m_b
95006	Jan. 6, 1995	22 37:37.9	40.227	142.242	57	6.7
95016	Jan. 16, 1995	18 14:49.4	51.241	179.172	33	5.5
95021	Jan. 21, 1995	08 47:29.9	43.335	146.717	63	6.5
95036	Feb. 5, 1995	22 51:10.4	-37.714	178.769	59	6.4
95045	Feb. 14, 1995	20 47:41.1	43.991	148.098	37	5.9
95090	March 31, 1995	14 01:40.8	38.150	135.058	365	6.0
95107	April 17, 1995	23 28:08.3	45.904	151.288	34	6.1
95111	April 21, 1995	00 09:56.2	11.999	125.699	33	6.1
95111	April 21, 1995	00 30:12.9	11.902	125.568	33	6.3
95113	April 23, 1995	05 08:03.2	12.377	125.364	33	6.0
95118	April 28, 1995	16 30:00.7	44.058	148.055	29	6.6
95119	April 29, 1995	09 44:00.3	11.766	126.044	33	5.4
95125	May 5, 1995	03 53:47.6	12.622	125.314	33	6.2
95128	May 8, 1995	18 08:09.6	11.567	125.900	33	5.6
95143	May 23, 1995	22 10:11.3	-56.097	-3.150	10	5.3
95175	June 24, 1995	06 58:06.5	-3.979	153.945	386	6.2
95180	June 29, 1995	07 45:09.7	48.784	154.459	62	5.9
95180	June 29, 1995	12 24:03.9	-19.464	169.241	144	6.2
95181	June 30, 1995	11 58:56.4	24.621	-110.264	10	5.8
95193	July 12, 1995	15 46:59.8	-23.237	170.824	33	5.9
95208	July 27, 1995	05 51:17.9	-12.578	79.237	10	6.2
95211	July 30, 1995	05 11:23.5	-23.364	-70.312	47	6.6
95215	Aug. 3, 1995	01 57:21.7	-23.132	-70.602	33	5.4
95226	Aug. 14, 1995	04 37:17.3	-4.827	151.507	126	6.3
95231	Aug. 19, 1995	21 43:32.4	5.096	-75.690	125	6.1
95235	Aug. 23, 1995	07 06:02.6	18.857	145.186	596	6.3
95257	Sept. 14, 1995	14 04:31.6	16.844	-98.599	21	6.4
95262	Sept. 19, 1995	03 31:53.6	-21.228	-68.740	110	5.7
95266	Sept. 23, 1995	22 31:58.3	-10.529	-78.697	73	5.9
95279	Oct. 6, 1995	18 09:45.9	-2.089	101.414	33	5.8
95291	Oct. 18, 1995	10 37:26.3	27.920	130.337	27	6.5
95292	Oct. 19, 1995	00 32:06.4	28.145	130.206	33	5.9
95305	Nov. 1, 1995	00 35:32.3	-28.958	-71.503	20	6.3
95312	Nov. 8, 1995	07 14:18.5	1.853	95.062	33	6.1
95328	Nov. 24, 1995	17 24:12.5	44.542	149.091	33	6.1
95331	Nov. 27, 1995	15 52:58.3	44.519	149.137	33	6.0
95334	Nov. 30, 1995	23 37:37.4	44.341	149.403	33	5.9
95336	Dec. 2, 1995	17 13:18.7	44.490	149.342	19	6.0
95337	Dec. 3, 1995	18 01:08.7	44.575	149.390	33	6.7
95345	Dec. 11, 1995	14 09:23.9	18.785	-105.505	33	5.7
95359	Dec. 25, 1995	04 43:24.9	-6.943	129.179	150	6.2
96001	Jan. 1, 1996	08 05:11.9	0.724	119.981	33	6.2
96038	Feb. 7, 1996	21 36:45.1	45.321	149.909	33	6.3
96047	Feb. 16, 1996	15 22:57.8	37.343	142.474	33	6.2
96053	Feb. 22, 1996	14 59:09.7	45.208	148.557	133	6.2
96065	March 5, 1996	14 52:28.6	24.092	122.215	30	6.1
96077	March 17, 1996	14 48:56.7	-14.705	167.297	164	5.8
96082	March 22, 1996	03 24:20.0	51.221	178.695	20	5.7
96090	March 30, 1996	13 05:17.4	52.214	-168.734	33	5.9
96107	April 16, 1996	00 30:54.6	-24.061	-177.036	111	6.4
96198	July 16, 1996	10 07:36.6	1.016	120.254	33	6.0
96204	July 22, 1996	14 19:35.7	1.000	120.450	33	6.0
96249	Sept. 5, 1996	23 42:06.1	21.898	121.498	20	6.4
96255	Sept. 11, 1996	02 37:14.9	35.537	140.943	55	6.1
96293	Oct. 19, 1996	08 31:49.8	31.840	131.804	33	5.4
96310	Nov. 5, 1996	09 41:34.7	-31.160	179.998	369	5.9
96357	Dec. 22, 1996	14 53:27.6	43.207	138.920	227	6.0
97023	Jan. 23, 1997	02 15:22.9	-21.999	-65.719	276	6.4
97084	March 25, 1997	16 44:32.5	-9.090	-71.320	603	5.4
97145	May 25, 1997	23 22:33.8	-31.980	179.700	333	7.1
97149	May 29, 1997	17 02:38.7	-35.964	-102.511	10	5.6

signal frequency. No significant variation of the parameters is observed, suggesting rather homogeneous anisotropic structures. However, the sensors band pass (0.1-10 Hz) impedes investigation on a broad range of periods, which could allow more reliable conclusions on the upper mantle heterogeneity.

The general coherency of the results allowed us to calculate the mean splitting parameters at each site. We used the averaging method presented by *Silver and* Chan [1991], which weights each individual measurement by its 95% confidence interval (reported in Table 3), so that poorly constrained results are have only a small contribution to the mean result. In order to test the validity of the result, we determined the mean splitting parameters (ϕ, δt) using three sets of data: (1) the whole set of measurements, (2) only good and fair measurements, and finally, (3) good measurements only. The results obtained from the three different data sets are consistent: ϕ and δt variations do not exceed ±5° and ±0.1 s, respectively. Therefore the mean splitting results presented in Table 1 and plotted in Figure 4 are based on the whole data set. GRF is the only station at which large variations in δt are observed depending on the averaged data: δt decreases from 1.75 s for the whole data set (14 measurements) to 1.56 s when four poor measurements with very high δt (above 2.0 s) are removed.

In the eastern part of the belt, most of the stations are characterized by a fast direction ϕ trending N90°E to N100°E and by rather high δt values in the range 1.0 to 1.7 s (see Table 1 and Figure 4). These results are generally well constrained by numerous splitting measurements. Except at station ORG, FNM, and BRU, average splitting parameters are calculated from more than five individual measurements and often from more than 10 measurements. No systematic variation of δt is observed across the belt, and particularly across the NPF, as in the central Pyrenees, indicating the absence of significant lateral variations in the anisotropy magnitude at depth. The ϕ trend observed at FNM in the Coastal Ranges (N120°E) seems to be slightly different than at the other stations, but it derives from a single measurement. No particularly strong δt is found at BSD, the station located close to the North Pyrenean Fault. Anisotropy in the southern Massif Central clearly contrasts with the rest of the profile, in trend, magnitude but also in quality. At FRS, the azimuth of the fast split shear wave trends around N75°E, the delay time seems to be significantly smaller than at the other stations (around 0.7 s), and some nulls are inconsistent with non-null splitting measurements. This pattern may be related to complex upper mantle structure beneath this station, such as dipping structures, heterogeneities, or multiple anisotropic layers.

In the western part of the belt, although the results derive from a much smaller data set, some high-quality events (see Figure 2) allow us to interpret the final results with confidence. The most striking feature is the homogeneity of the results across the belt: ϕ trends around N110°E and δt is homogeneously high, around 1.3 to 1.4 s. As in the eastern Pyrenees, no specific anisotropy signature is observed at the station closest to the NPF (LAR).

The anisotropy study in the central Pyrenees [*Barruol and Souriau*, 1995] led to the main following results: (1) the anisotropy in the Pyrenean units belonging to the Iberian plate is homogeneous with splitting parameters, $\phi \approx$ N100°E and δt in the range 1.3 to 1.5 s. (2) North from the NPF, anisotropy in the North Pyrenean Zone is characterized by varying ϕ (from N70°E to E-W) and smaller δt (0.6 to 1.0 s).

Splitting measurements obtained from the three profiles,

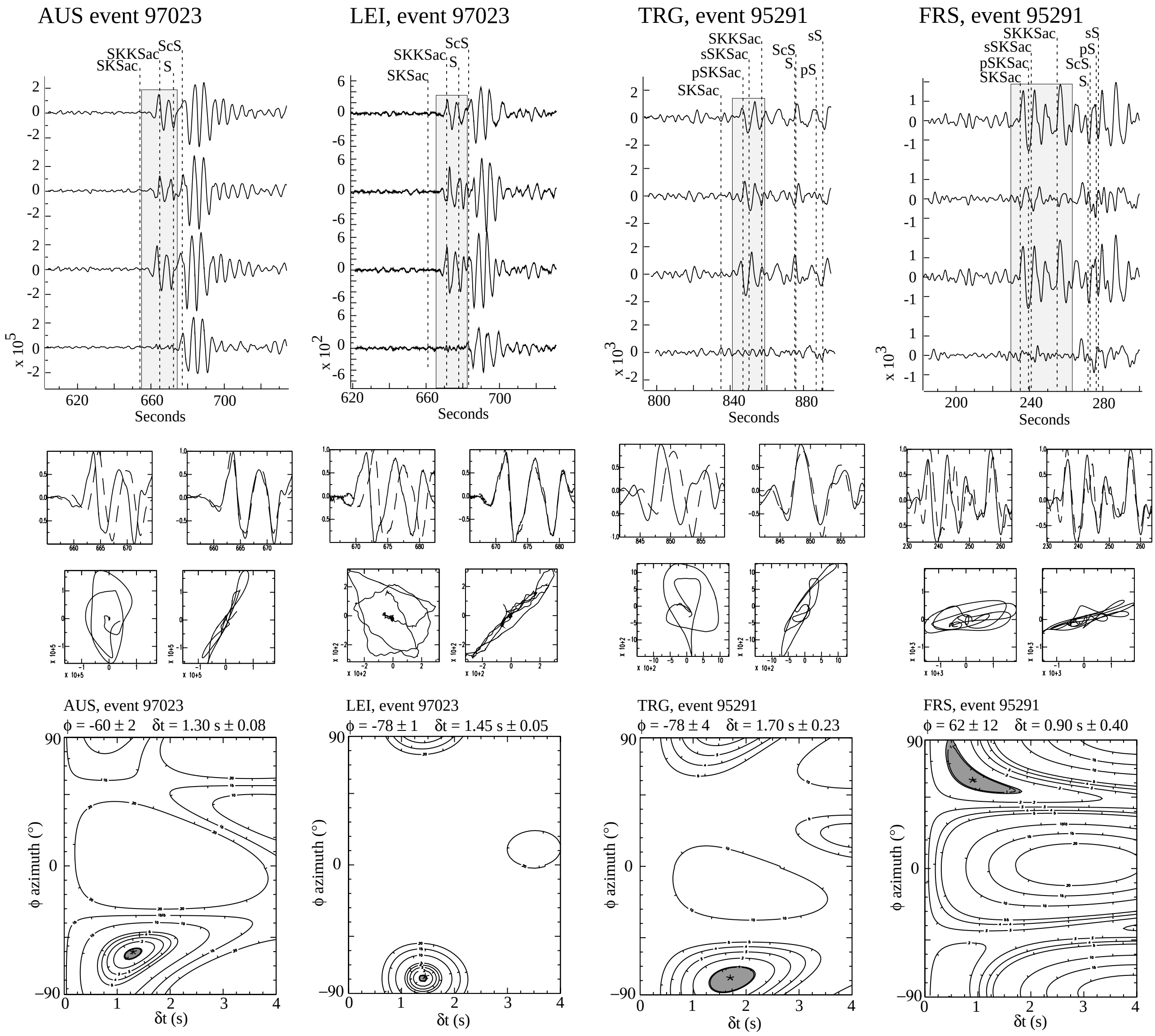

Figure 2. Examples of splitting measurements at four stations: *SKS* phase for event 97023 (see location on Table 2), recorded at two stations from the western Pyrenees (AUS and LEI) on both sides of the North Pyrenean Fault, and event 95291, recorded at two stations from the eastern experiment, one in the axial zone (TRG) and the other in the southern Massif Central (FRS). (top) For each station we show two upper traces, the initial radial and transverse components (note the energy on the transverse component), and two lower traces, the same traces corrected for anisotropy (there is no longer energy on the transverse component). The vertical dashed lines represent the predicted phase arrival times from the IASP91 Earth model. The shaded area gives the time window on which the splitting measurement is done. (middle) Four plots of the fast and slow components (continuous and dashed lines, respectively) of the split shear waves, (left) raw and (right) corrected for the best calculated delay time. Particle motions in the horizontal plane are shown below, also (left) uncorrected and (right) corrected for the anisotropy: the elliptical particle motion becomes rectilinear when the anisotropy is corrected. (bottom) Contour plot of energy on the transverse component as a function of the delay time δt (seconds) and the polarization angle ϕ (degrees) of the fast split shear wave. The shaded area represents the 95% confidence interval. This last diagram allows the determination of 95% confidence interval for the splitting parameters from which the 1σ uncertainties are deduced.

together with those obtained at the NARS station NE10 [*Souriau and Njike-Kassala*, 1993], allow us to define some general characteristics: On the Iberian plate, ϕ homogeneously trends around N100-110°E, and δt is rather large, typically in the range 1.1 to 1.5 s. On the other hand, the abrupt variation in splitting parameters across the North Pyrenean Fault observed in the central Pyrenees is not observed in the eastern and western portions of the belt. Instead, ϕ is rather stable along the eastern profile (around N100°E) except for stations out of the range (FRS in the Massif Central and FNM in the Catalan Coastal ranges). Interestingly, GRF, also out of the range has one of the highest δt of the profile (1.75 s).

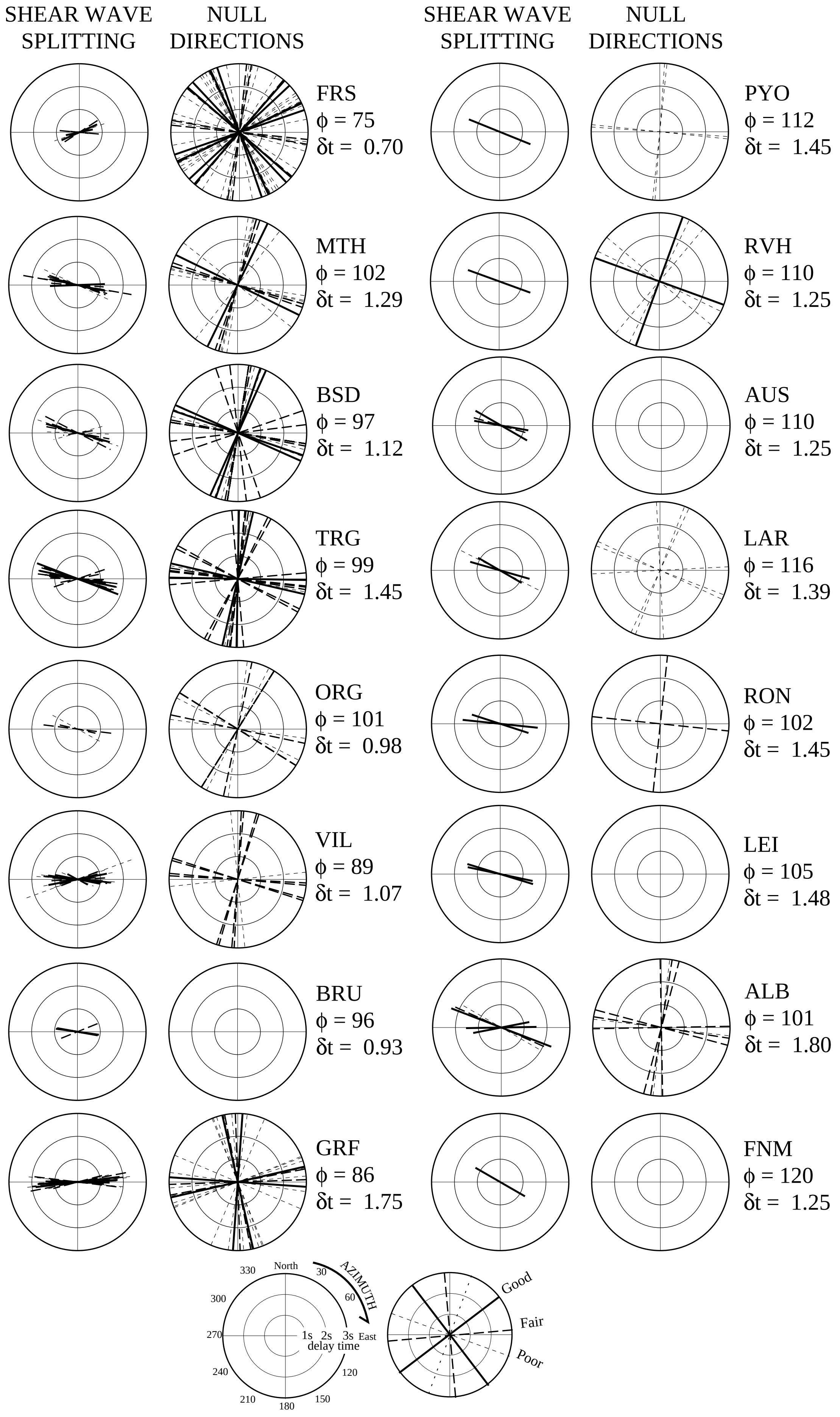
SHEAR WAVE SPLITTING
NULL DIRECTIONS
SHEAR WAVE SPLITTING
NULL DIRECTIONS
FRS
ϕ = 75
δt = 0.70
PYO
ϕ = 112
δt = 1.45
MTH
ϕ = 102
δt = 1.29
RVH
ϕ = 110
δt = 1.25
BSD
ϕ = 97
δt = 1.12
AUS
ϕ = 110
δt = 1.25
TRG
ϕ = 99
δt = 1.45
LAR
ϕ = 116
δt = 1.39
ORG
ϕ = 101
δt = 0.98
RON
ϕ = 102
δt = 1.45
VIL
ϕ = 89
δt = 1.07
LEI
ϕ = 105
δt = 1.48
BRU
ϕ = 96
δt = 0.93
ALB
ϕ = 101
δt = 1.80
GRF
ϕ = 86
δt = 1.75
FNM
ϕ = 120
δt = 1.25
North
30
60
East
120
150
180
210
240
270
300
330
AZIMUTH
1s
2s
3s
delay time
Good
Fair
Poor

3. The Lithospheric Origin of the Anisotropy

Although it is widely accepted that a major part of the teleseismic shear wave splitting occurs in the upper mantle, the lack of vertical resolution in measurements of core shear waves splitting let open the investigations about the asthenospheric and/or lithospheric origin of the splitting. Inferences about the source regions of anisotropy and the processes that generate mantle deformation fabrics may be drawn through a comparison of anisotropy signatures expected from these processes and observed splitting parameters.

In the central Pyrenees, the short-scale variation of the anisotropy parameters and their correlation to the NPF, as well as the better correlation of the azimuth of the fast split direction with lithospheric structures rather than with absolute plate motion orientation, led *Barruol and Souriau* [1995] to suggest that the anisotropy is predominantly of lithospheric origin.

In light of the new data presented in this work, this discussion has to be updated. We first compare our observations with the anisotropy predicted from absolute plate motion (APM). Assuming a flat geometry of the lithosphere/asthenosphere boundary, asthenospheric drag beneath a lithospheric plate would result in ϕ oriented parallel to the plate motion vector [*Tommasi et al*., 1996; *Vinnik et al*., 1992]. The HS2-Nuvel1 and NNR-Nuvel1 absolute plate motion models predict asthenospheric flow beneath the Pyrenees trending about N45°-N50°E [*DeMets et al*., 1990; *Gripp and Gordon*, 1990]. These predictions, however, are poorly constrained for the Eurasian plate because of the very low velocity of this plate and because no local hot spot tracks were incorporated into the HS2-Nuvel1 model to constrain local APM. J. Morgan (personal communication, 1996) defined a model incorporating hot spot tracks on the Eurasian and African plates which gives a APM trending N80°E with a velocity of about 5 mm/yr in the Pyrenees. Excepted for the Massif Central station FRS, none of the measured fast polarization direction is close to the prediction for any model. The misfit reaches 20-30° using Morgan's APM and 50 to 60° using HS2-Nuvel1 APM. Second, short-wavelength variations in the splitting parameters found in several places in the eastern Pyrenees are hardly compatible with a deep source (deeper than 100 km) of anisotropy related to large-scale mantle shear flow. For instance, significant δt variations are observed between TRG (δt = 1.45 s) and VIL (δt = 1.07 s) less than 50 km apart. Third, the observed ϕ directions correlate well with the outcropping lithospheric structures: ϕ is parallel to the Pyrenean and Hercynian pervasive structures of the Pyrenees. Fourth, the largest δt are generally observed on the Iberian plate, which was found, from *P* wave residuals [*Poupinet et al*., 1992], to have a thicker crust and lithosphere than the adjacent European plate. This apparent correlation of δt with lithospheric thickness is compatible with a lithospheric origin of the anisotropy. Fifth, it is also interesting to note that *Pn* tomography [*Granet et al*., 1997] reveals a *P* wave anisotropy of about 4% trending roughly E-W in the central and eastern Pyrenees. This fast *P* wave direction in the uppermost lithospheric mantle is compatible with our *SKS* splitting observations and clearly argue for a subcrustal, lithospheric anisotropy.

More complex asthenospheric models of forced flow around complex geometry of the lithosphere-asthenosphere boundary have been suggested [*Bormann et al*., 1996] to integrate short-scale anisotropy variations in an asthenospheric mantle flow. The tomographic studies [*Souriau and Granet*, 1995], *P* residuals [*Poupinet et al*., 1992] or electromagnetic soundings [*Pous et al*., 1995] support the existence of a downward lithospheric bending of the Iberian lithosphere but do not give evidence of short-wavelength sublithospheric heterogeneities.

Observations in the eastern and western Pyrenees therefore strengthen the previous conclusions inferred from the central Pyrenees measurements, that is, that the anisotropy appears to correlate better with the uppermost mantle structures rather than with an asthenospheric flow beneath the plate. Obviously, this latter contribution cannot be reasonably rejected from our observations, but if present, it seems to be much smaller than the lithospheric effect.

4. Seismic Anisotropy and Deep Structures of the Belt

Considering that uppermost mantle structures dominates our shear wave splitting measurements in the Pyrenees, it is worth comparing our results to other geophysical data available for this belt. At the crustal scale, an asymmetric structure of the belt is well established by various methods, particularly for the central Pyrenees: balanced cross sections [*Séguret and Daignières*, 1986] show that the Iberian crust was much thicker than the Eurasian margin after the rotation of Iberia 107-90 Myr ago. This N-S crustal asymmetry is still present as imaged from seismic refraction profiles [*Daignières et al*., 1982] and has been largely confirmed by the ECORS vertical seismic reflection experiment [*Roure and ECORS Pyrenees Team*, 1989]. In the central part of the range, the Iberian crust is 15 km thicker than the Eurasian crust.

The N-S asymmetry of the belt has also been imaged at lithospheric scale in the central Pyrenees. Interpretation of *P* travel time residuals [*Poupinet et al*., 1992] confirms the large Moho vertical offset and also suggests an Iberian lithosphere thicker than the Eurasian one. The seismic tomography of the belt [*Souriau and Granet*, 1995] reveals, at upper mantle depths (between 50 and 100 km) beneath the Pyrenean Axial Zone (see Figure 5a), a prominent E-W trending low-velocity anomaly, contrasting with high velocities observed beneath the NPZ and Aquitaine Basin. This anomaly was interpreted as an incipient subduction of Iberian lower crust beneath the Eurasian plate. A similar conclusion was reached independently by *Pous et al*. [1995] from magnetotelluric soundings along a N-S profile in the

Figure 3. (opposite) Summary of (left) non-null and (right) null measurements at each station. For non-null measurements, the trend of each segment represents the azimuth of the fast split shear wave polarization plane, and its length is proportional to the delay time (up to 3.0 s). Solid lines correspond to well-constrained results, large dashed lines correspond to fair results, and small dashed lines correspond to poorly constrained results (as reported Table 3). For null measurements, we represents backazimuth (radial direction) of unsplit events. We also plot the perpendicular (transverse) direction that may correspond to the fast or slow direction in the anisotropic layer. For each station, we report the calculated splitting parameters.

Table 3. Results of Individual Splitting Measurements Obtained at Various Stations

Station	Event	Distance, deg	Back-azimuth, deg	ϕ, deg	$\sigma\phi$, deg	δt, s	$\sigma\ \delta t$, s	Phase	Quality
FRS	95006	89	30	-84.	-	-	-	*SKS*	f
FRS	95016	91	38	-26.	-	-	-	*SKS*	f
FRS	95107	87	21	40.	-	-	-	*SKS*	f
FRS	95111	105	58	-84.	18.	0.40	0.22	*SKS*	f
FRS	95113	104	58	71.	7.	1.15	0.32	*SKS*	p
FRS	95119	105	58	-26.	-	-	-	*SKKS*	f
FRS	95175	133	41	-43.	-	-	-	*PKS*	g
FRS	95180	154	29	-79.	-	-	-	*SKKS*	p
FRS	95211	94	242	-33.	-	-	-	*SKS*	p
FRS	95215	94	242	65.	-	-	-	*SKS*	g
FRS	95226	133	44	78.	6.	0.60	0.10	*PKS*	g
FRS	95228	135	42	55.	-	-	-	*PKS*	p
FRS	95266	91	256	71.	-	-	-	*SKS*	g
FRS	95291	94	44	66.	11.	0.85	0.30	*SKS*	g
FRS	95291	94	44	57.	13.	0.95	0.40	*SKKS*	f
FRS	95312	91	87	-80.	-	-	-	*SKS*	f
FRS	95337	88	23	-49.	-	-	-	*SKS*	g
FRS	96064	93	53	60.	-	-	-	*SKS*	p
FRS	96076	149	29	-85.	14.	0.86	0.34	*SKKS*	f
FRS	95021	88	25	-82.	-	-	-	*SKS*	p
FRS	95128	105	58	-57.	-	-	-	*SKS*	p
FRS	95279	98	85	-74.	-	-	-	*SKS*	p
FRS	95292	94	44	-23.	-	-	-	*SKS*	p
FRS	95305	99	238	-27.	-	-	-	*SKS*	p
FRS	95334	88	23	79.	-	-	-	*SKS*	p
MTH	95006	90	30	-77.	-	-	-	*SKS*	p
MTH	95053	87	23	16.	-	-	-	*SKS*	f
MTH	95090	88	35	-74.	3.	1.35	0.18	*SKS*	f
MTH	95111	105	58	-65.	9.	1.60	0.35	*SKS*	p
MTH	95111	105	58	-71.	4.	1.30	0.13	*SKS*	f
MTH	95113	104	58	-86.	6.	1.15	0.18	*SKS*	f
MTH	95118	88	24	-52.	-	-	-	*SKS*	p
MTH	95125	104	58	-78.	6.	1.25	0.18	*SKS*	g
MTH	95128	105	58	-79.	4.	1.35	0.13	*SKS*	p
MTH	95143	99	183	14.	-	-	-	*SKS*	p
MTH	95175	134	41	88.	8.	1.20	0.23	*PKS*	g
MTH	95175	134	41	-79.	8.	1.50	0.33	*SKKS*	p
MTH	95181	89	43	-80.	4.	2.40	0.30	*SKS*	f
MTH	95215	94	242	-74.	10.	0.90	0.18	*SKS*	f
MTH	95226	133	44	-90.	9.	1.10	0.20	*PKS*	p
MTH	95331	88	23	19.	-	-	-	*SKS*	f
MTH	95334	87	26	-81.	-	-	-	*SKS*	p
MTH	95337	88	23	-64.	-	-	-	*SKS*	g
MTH	96053	87	23	16.	-	-	-	*SKS*	f
MTH	96107	161	359	-74.	-	-	-	*SKKS*	p
BSD	95006	90	29	-72.	3.	1.85	0.43	*SKS*	p
BSD	95111	105	58	-63.	6.	1.60	0.23	*SKS*	f
BSD	95113	105	58	-71.	13.	1.20	0.25	*SKKS*	f
BSD	95118	88	24	71.	-	-	-	*SKS*	f
BSD	95175	134	41	81.	8.	0.65	0.13	*PKS*	f
BSD	95180	86	18	-66.	-	-	-	*SKS*	g
BSD	95211	94	241	83.	-	-	-	*SKKS*	f
BSD	95215	94	242	-71.	-	-	-	*SKS*	g
BSD	95215	94	242	-76.	-	-	-	*SKS*	p
BSD	95231	78	266	9.	-	-	-	*SKS*	f
BSD	95235	110	37	-82.	10.	0.70	0.15	*SKS*	p
BSD	95235	110	37	75.	4.	1.10	0.13	*SKSdf*	p
BSD	95257	86	290	-81.	-	-	-	*SKS*	f
BSD	95262	91	242	-88.	4.	1.35	0.18	*SKS*	p
BSD	95291	95	44	-74.	12.	1.45	0.45	*SKS*	g
BSD	95331	88	23	-70.	-	-	-	*SKS*	p
BSD	95334	87	26	-81.	-	-	-	*SKS*	p
BSD	95337	88	23	-79.	-	-	-	*SKS*	f
BSD	95359	122	68	-77.	9.	0.90	0.18	*SKKS*	f
BSD	96053	87	23	-81.	-	-	-	*SKS*	f
BSD	96065	94	52	-79.	4.	1.40	0.15	*SKS*	f

Table 3. (continued)

Station	Event	Distance, deg	Back-azimuth, deg	ϕ, deg	$\sigma\phi$, deg	δt, s	$\sigma\ \delta t$, s	Phase	Quality
TRG	95006	90	29	-79.	-	-	-	*SKS*	p
TRG	95107	88	21	29.	-	-	-	*SKS*	f
TRG	95111	105	57	-69.	3.	1.90	0.15	*SKS*	g
TRG	95113	105	57	-71.	5.	1.55	0.18	*SKS*	g
TRG	95122	84	260	-85.	9.	1.25	0.38	*SKS*	f
TRG	95125	105	57	-78.	2.	1.75	0.10	*SKS*	f
TRG	95128	106	57	-83.	6.	1.75	0.28	*SKS*	p
TRG	95175	134	41	-77.	14.	0.75	0.30	*PKS*	f
TRG	95175	134	41	-73.	3.	1.65	0.15	*SKKS*	f
TRG	95180	86	18	7.	-	-	-	*SKS*	f
TRG	95181	89	302	78.	15.	0.95	0.30	*SKS*	p
TRG	95193	159	29	-88.	12.	1.20	0.35	*SKKS*	f
TRG	95208	89	108	26.	-	-	-	*SKKS*	f
TRG	95215	93	242	85.	-	-	-	*SKS*	f
TRG	95231	78	265	1.	-	-	-	*sSKS*	g
TRG	95266	90	256	-81.	5.	1.25	0.20	*SKS*	g
TRG	95291	95	44	-78.	4.	1.70	0.23	*SKS*	g
TRG	95305	98	238	71.	4.	1.25	0.30	*SKS*	f
TRG	95337	89	23	-77.	-	-	-	*SKS*	g
TRG	95359	122	68	-77.	10.	0.70	0.17	*SKKS*	f
TRG	96053	88	23	-84.	-	-	-	*SKS*	f
TRG	96065	94	52	-83.	6.	1.45	0.18	*SKS*	f
TRG	96077	150	29	-83.	2.	1.75	0.13	*SKKS*	f
TRG	96106	162	357	9.	-	-	-	*SKS*	f
VIL	95107	88	21	69.	11.	0.95	0.23	*SKS*	f
VIL	95111	105	57	-79.	8.	1.00	0.15	*SKS*	g
VIL	95111	105	57	-84.	6.	1.40	0.20	*SKS*	f
VIL	95113	105	57	-85.	8.	1.50	0.30	*SKS*	f
VIL	95125	105	57	-86.	6.	1.10	0.18	*SKS*	g
VIL	95128	106	57	-67.	20.	0.75	0.38	*SKS*	p
VIL	95193	159	30	-83.	9.	1.60	0.40	*SKKS*	p
VIL	95215	93	242	79.	9.	1.55	0.58	*SKS*	p
VIL	95226	134	45	85.	9.	0.80	0.23	*PKS*	f
VIL	95231	77	265	-85.	-	-	-	*sSKS*	f
VIL	95257	86	289	84.	-	-	-	*SKS*	p
VIL	95266	103	86	-82.	4.	1.30	0.35	*SKS*	f
VIL	95266	90	256	-64.	14.	0.50	0.13	*SKS*	f
VIL	95279	98	85	-61.	21.	0.50	0.35	*SKS*	f
VIL	95291	96	44	79.	10.	1.30	0.25	*SKS*	g
VIL	95292	95	44	70.	7.	2.5	0.40	*SKS*	p
VIL	95292	95	44	75.	5.	0.90	0.10	*SKS*	f
VIL	95305	98	238	71.	6.	1.25	0.38	*SKS*	p
VIL	95312	91	87	16.	-	-	-	*SKS*	f
VIL	95359	122	68	-82.	6.	0.80	0.13	*SKS*	g
VIL	96065	94	52	87.	7.	1.20	0.23	*SKS*	f
VIL	96077	150	29	-86.	5.	1.80	0.30	*SKKS*	p
VIL	96082	87	2	18.	-	-	-	*SKS*	f
VIL	96107	162	357	3.	-	-	-	*SKKS*	f
GRF	95107	89	21	79.	5.	2.15	0.30	*SKS*	f
GRF	95111	106	58	83.	4.	1.85	0.28	*SKS*	g
GRF	95113	106	58	85.	-	-	-	*SKS*	p
GRF	95118	90	24	-22.	-	-	-	*SKS*	p
GRF	95125	105	58	-89.	3.	1.40	0.10	*SKS*	g
GRF	95143	97	183	78.	-	-	-	*SKS+SKKS*	p
GRF	95175	135	42	75.	5.	1.10	0.15	*PKS*	f
GRF	95180	156	30	85.	4.	2.15	0.13	*SKKS*	p
GRF	95180	87	18	87.	4.	1.75	0.30	*SKS*	g
GRF	95193	160	31	-84.	3.	2.15	0.18	*SKKS*	p
GRF	95199	89	108	88.	-	-	-	*SKS*	f
GRF	95211	93	241	72.	-	-	-	*SKS*	p
GRF	95215	93	242	-85.	17.	1.20	0.45	*SKS*	f
GRF	95226	135	45	77.	7.	1.40	0.23	*PKS*	p
GRF	95226	135	45	-67.	-	-	-	*SKS*	p
GRF	95231	77	266	79.	-	-	-	*SKS*	f
GRF	95231	77	266	4.	-	-	-	*sSKS*	g
GRF	95266	90	256	-87.	6.	1.15	0.25	*SKS*	g

Table 3. (continued)

Station	Event	Distance, deg	Back-azimuth, deg	ϕ, deg	$\sigma\phi$, deg	δt, s	$\sigma\ \delta t$, s	Phase	Quality
GRF	95291	97	44	-83.	8.	1.90	0.40	*SKS+SKKS*	f
GRF	95305	97	238	88.	7.	1.70	0.30	*SKS*	f
GRF	95337	90	22	84.	3.	2.00	0.23	*SKS*	f
GRF	96001	111	70	77.	-	-	-	*SKS*	g
GRF	96038	89	22	69.	-	-	-	*SKS*	p
GRF	96077	151	29	84.	3.	2.30	0.10	*SKKS*	p
GRF	96090	87	354	-86.	-	-	-	*SKS*	f
GRF	96107	163	356	-82.	-	-	-	*SKKS*	p
ORG	95036	175	24	8.	-	-	-	*SKKS*	p
ORG	95107	88	21	-83.	5.	1.50	0.40	*SKS*	f
ORG	95118	89	23	-78.	-	-	-	*SKS*	f
ORG	95291	96	44	-61.	11.	1.25	0.46	*SKS*	p
ORG	95304	98	46	-77.	7.	0.80	0.10	*SKS*	f
ORG	95336	89	22	32.	-	-	-	*SKS*	f
ORG	95337	89	22	-58.	-	-	-	*SKS*	f
ORG	96038	88	22	32.	-	-	-	*SKS*	f
ORG	96065	94	52	-63.	-	-	-	*SKS*	p
BRU	95036	175	30	68.	16.	0.95	0.28	*SKKS*	f
BRU	95111	105	58	-80.	10.	0.90	0.18	*SKS*	g
BRU	95111	105	58	-82.	3.	0.95	0.08	*SKS*	g
FNM	95111	105	58	-60.	5.	1.25	0.18	*SKS*	g
ALB	95111	105	58	-66.	3.	2.20	0.15	*SKS*	f
ALB	95257	87	290	-81.	-	-	-	*SKS*	f
ALB	95266	102	87	-60.	11.	1.9	0.29	*SKKS*	p
ALB	95266	102	87	89.	6.	1.54	0.48	*SKS*	g
ALB	95279	98	86	-68.	10.	1.06	0.27	*SKKS*	f
ALB	95291	95	45	-69.	2.	2.34	0.18	*SKS*	g
ALB	95305	98	239	79.	3.	1.25	0.16	*SKS*	g
ALB	95336	89	23	89.	-	-	-	*SKS*	f
ALB	95337	89	23	-83.	-	-	-	*SKS*	p
ALB	96053	88	23	-75.	-	-	-	*SKS*	f
LAR	96198	112	67	-65.	-	-	-	*SKS+SKKS*	p
LAR	96204	112	67	87.	-	-	-	*SKS+SKKS*	p
LAR	96249	97	52	-60.	3.	1.10	0.15	*SKS*	g
LAR	96255	94	30	-69.	-	-	-	*SKS*	p
LAR	96293	94	39	-74.	7.	1.35	0.25	*SKS*	g
LAR	96310	168	356	-63.	4.	1.90	0.25	*SKKS*	p
AUS	96357	87	28	-80.	2.	1.20	0.13	*SKS*	g
AUS	97023	88	237	-60.	2.	1.30	0.08	*SKS*	g
AUS	97084	82	250	-74.	10.	1.25	0.95	*S(609km)*	f
RVH	96249	96	52	40.	-	-	-	*SKKS*	p
RVH	96293	93	39	-70.	-	-	-	*SKS*	g
RVH	96357	87	28	-70.	2.	1.45	0.23	*SKS*	g
RVH	97149	121	249	-64.	-	-	-	*SKS*	p
PYO	96293	93	39	-68.	5.	1.45	0.28	*SKS*	g
PYO	96357	86	28	-84.	-	-	-	*SKS*	p
PYO	97145	168	358	4.	-	-	-	*SKKS*	p
LEI	96357	87	28	-73.	2.	1.50	0.20	*SKS*	g
LEI	97023	87	237	-78.	1.	1.45	0.05	*SKS*	g
RON	96357	87	28	-84.	4.	1.65	0.23	*SKS*	g
RON	97145	169	357	-84.	-	-	-	*SKS*	f
RON	97145	169	357	-72.	4.	1.30	0.15	*SKKS*	g

The shear phase is indicated together with a quality of the measurements (g, good; f, fair; p, poor). For "null" results (events for which no signal has been found on the transverse component) only the distance and backazimuth are reported.

central Pyrenees. Their observations revealed a highly conductive body beneath the Pyrenean Axial Zone down to 80 km depth, which contrasts with a highly resistive upper mantle farther north. They interpret this anomaly as subducted crustal material, with possible partial melt beneath the PAZ. Some interesting features appear combining our shear wave splitting observations with upper mantle seismic tomography results (Figure 5a). In the central and eastern Pyrenees, large δt are observed at stations located above the low-velocity anomaly in the upper mantle, whereas smaller values are observed at the periphery. This could suggest that dipping lithospheric material, for which the crustal part only is visible in tomographic maps, is responsible for the large splitting. However, in western Pyrenees, where no subduction took place, large δt values are also observed. Thus another explanation has to be found. The splitting parameter pattern, however, confirms the departure from cylindrical symmetry previously observed from other geophysical data.

An E-W elongated negative Bouguer gravity anomaly [*Casas et al*., 1997; *De Cabissole*, 1989; *Grandjean*, 1994; *Torne et al*., 1989] beneath the Axial and South Pyrenean Zone (Figure 5b) is consistent with an abnormally thick Iberian crust. High positive Bouguer anomalies in the North Pyrenean Zone are likely related to a thinner Eurasian crust and to mantle intrusions within the crust along the belt; some of the latter are observed in crustal seismic tomography studies [*Grandjean*, 1994; *Souriau and Granet*, 1995]. Combining anisotropy information together with the Bouguer anomaly map (Figure 5b) does not reveal any significant correlation, indicating that the source of anisotropy is located beneath the source of this gravimetric anomaly, i.e., at subcrustal levels. This is true even for stations located at the two prominent gravity anomalies ("Saint Gaudens" and "Labourd" anomalies) in the western and central Pyrenees, which are interpreted as due to the presence of an upper mantle body at crustal depth [*Grandjean*, 1994; *Torne et al*., 1989].

5. Tectonic Origin of Anisotropy

The tectonic evolution of the Pyrenean domain was long lasting and continues today. Several deformation episodes may have contributed to the lithospheric fabric responsible for seismic anisotropy. Possible origins of anisotropy are discussed from present-day to past tectonic processes: today's state of stress, pervasive deformation related to the Pyrenean orogeny and pre-Pyrenean pervasive structures.

5.1. Stress-Induced Anisotropy and Crustal Contribution to Shear Wave Splitting

Microcrack-induced anisotropy [*Crampin*, 1984] may explain delay times of a few tenths of seconds and is generally correlated to the state of stress in the upper crust. The present-day state of stress in the Pyrenees is characterized by rather complex pattern. The world stress map [*Zoback*, 1992] shows maximum horizontal stress directions in the western Pyrenees varying from NW-SE to NE-SW over short distances. Regional earthquake focal mechanisms [*Delouis et al*., 1993; *Rigo et al*., 1997] indicate a complex stress field in the Pyrenees. Interpolation of the stress data in France provided by *Rebai et al*. [1992] seems however to indicate a maximum horizontal compressive direction oriented roughly N-S in the eastern and central Pyrenees and NW-SE in the western Pyrenees. Assuming a stress-controlled anisotropy, the fast split shear waves should parallel open microcracks and

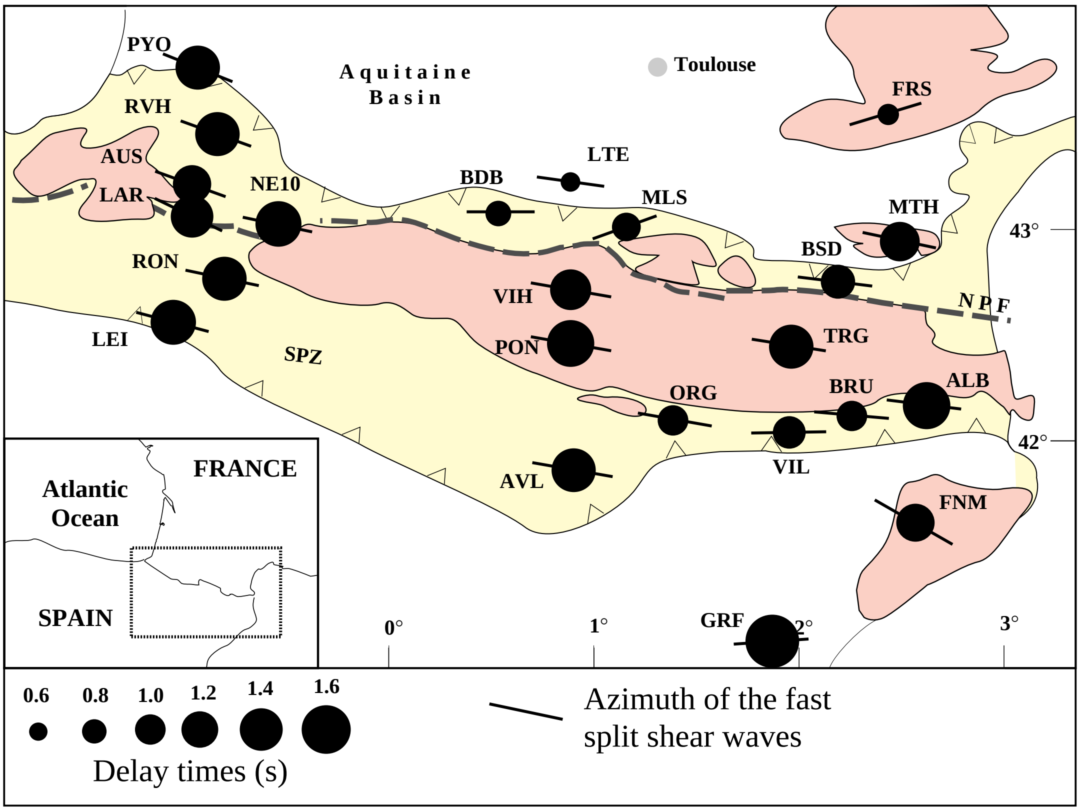

Figure 4. Map of the *SKS* splitting results in the Pyrenees from this study (in the eastern and western Pyrenees), from *Barruol and Souriau* [1995] in the central Pyrenees, and from *Souriau and Njike-Kassala* [1993] for the NARS station NE10. For each station, the mean value deduced from individual splitting measurements is represented by a circle whose radius is proportional to δt; the solid segment represents the azimuth of the fast direction ϕ.

therefore the trend of maximum compression direction, a situation which is clearly not observed. From the lack of correlation of the anisotropy with present-day stress field in the Pyrenees, we conclude that microcracks-induced anisotropy in the upper crust does not dominate the observed shear wave splitting. The N-S direction of compression observed in the crust reflects the present-day convergence of the plates. At upper mantle level, this compression may currently produce an E-W trending fabric, compatible with our measurements. We discuss these possible processes in section 5.3.

Lower crustal shear wave splitting is difficult to detect, but several studies [e.g., *Herquel et al.*, 1995; *McNamara and Owens*, 1993] indicate that 0.1 to 0.3 s delay times could be attributed to pervasive lower crustal fabric. These observations are in agreement with petrophysical predictions based on typical crustal fabrics that lead to delay times of around 0.1 s per 10 km thickness of anisotropic medium [*Barruol and Mainprice*, 1993]. In summary, the crust likely contributes to the total splitting (up to 10 to 20% of the observed delays) but cannot alone explain our observations (delay times higher than 1 s and often around 1.5 s).

5.2. Paleogene and Neogene Deformations in the Catalan Coastal Ranges

The Miocene opening of the western Mediterranean basin (21 Ma) was preceded by Oligocene extensional tectonics (25 Ma) along the northeastern part of the Iberian continental margin where two of our stations (FNM and GRF) are located. This extension created the Valencia trough, southeast of Barcelona [*Banda and Santanach*, 1992] and induced the uplift of the rift's shoulder and the formation of the Catalan coastal ranges (Figure 1). The related crustal thinning is well imaged by seismic reflection profiling of the Iberian margin [e.g., *Gallart et al.*, 1994] that shows a crustal thickness reduced from 30 to 15 km over a few tenths of a kilometer offshore. Crustal extensional structures exposed in the Catalan coastal ranges are NE-SW trending grabens associated to NW-SE transcurrent faults [*Vegas*, 1992]. Although crustal thinning related to the Valencia trough opening seems to be restricted offshore, the Miocene paleostress directions as deduced from brittle structures onshore are consistent with an EW to NW-SE direction of extension [*Bartrina* et al., 1992].

Assuming coherent deformation of the lithosphere, the upper mantle stretching related to this tectonic episode beneath the Catalan coastal ranges should result in a shallow to moderately dipping foliation and in an E-W to NW-SE trending flow direction (lineation). The corresponding anisotropy should trend parallel to the flow direction. Our observations at FNM (ϕ = N120° but deduced from a single measurement) and at GRF (ϕ = N86°) may be compatible with such a trend. However, upper mantle xenolith seismic properties are such that a flat-lying foliation is weakly anisotropic (< 2%) for a vertically propagating shear wave [*Ji et al.*, 1994; *Mainprice and Silver*, 1993]. The strong anisotropy recorded at GRF (δt = 1.75 s) is therefore hardly compatible with this explanation alone. A Miocene anisotropy may be superimposed on the Hercynian fabrics at the base of the lithosphere on the eastern edge of the Pyrenees but two anisotropies of different ages with similar orientations cannot be distinguished by the method. However, the homogeneity of the

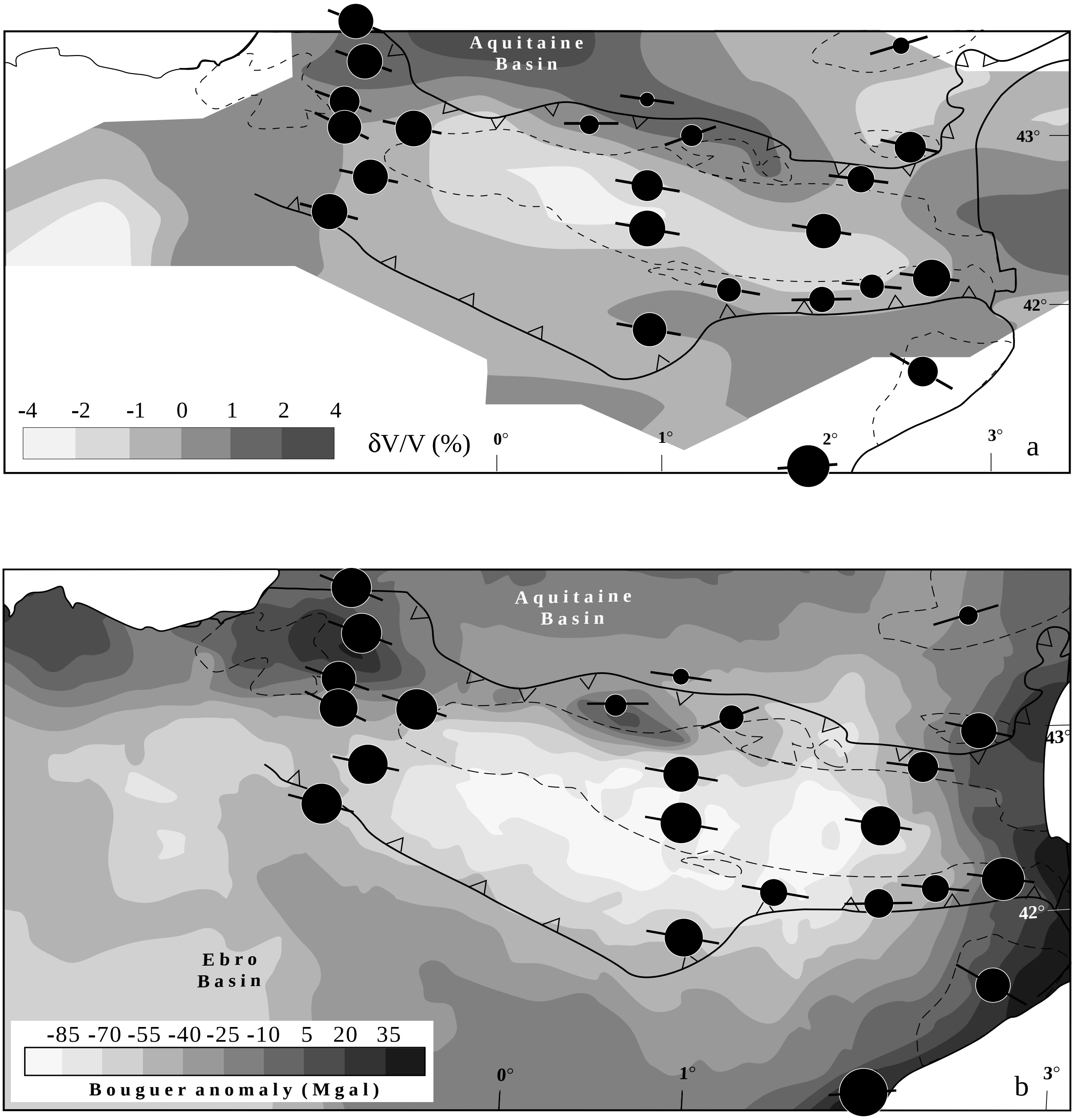

Figure 5. Map of *SKS* splitting results in the Pyrenees superimposed on (a) *P* wave velocity heterogeneity at depth of 50 to 100 km from *Souriau and Granet* [1995]. The low-velocity body beneath the axial zone is interpreted as Iberian lower crust subduction. (b) Bouguer anomaly adapted from *Grandjean* [1992] and *De Cabissole* [1989]. Note the low and broad anomaly parallel to the trend of the belt corresponding to the Iberian crust thickening toward the north and the high anomalies in the NPZ corresponding likely to upper mantle bodies at crustal depth.

results obtained in the eastern Pyrenees with those obtained from the central and western profiles suggests that extension-related fabric does not dominate the signal.

5.3. Pyrenean Anisotropy

The Pyrenean orogeny can be divided into two distinct phases: (1) rotation of Iberia with respect to Eurasia during Albian-Cenomanian times (100 Ma) that resulted in a large left-lateral strike-slip motion and in the thinning of the Eurasian margin. Related to this tectonic episode is a mantle upwelling responsible for both emplacement of the upper mantle slices in the shallow crust [*Vielzeuf and Kornprobst*, 1984] and high-temperature metamorphism [*Golberg and Leyreloup*, 1990] affecting the rift sediments (the present-day North Pyrenean Zone); (2) N-S collision that began at late Cretaceous (about 80 Ma) but culminated during Eocene times, about 45 Ma [e.g., *Choukroune*, 1992]. From the plate reconstruction [*Choukroune*, 1992; *Olivet*, 1996], the total strike-slip displacement is estimated around 200-300 km, and the proposed N-S shortening during the collision between the two plates is probably around 100 km. Figure 6 shows a possible interpretation of the origin of the anisotropy through successive cartoons from late Hercynian event to present-day situation.

During the Albian-Cenomanian strike-slip motion of the plates, the lithosphere is extremely thinned, and the flow direction in the asthenospheric mantle wedge beneath the rifted domain is expected to be roughly parallel to the rift direction (Figure 6b). The narrowness (less than 20 km) of the domain affected by crustal deformation and high-temperature metamorphism suggests that the upper mantle rifted zone is narrow too. Taking into account upper mantle seismic properties determined from xenolith studies [*Ben Ismail and Mainprice*, 1998; *Ji et al.*, 1994; *Mainprice and Silver*, 1993], the related anisotropy at that stage is expected to be characterized by a ϕ trending parallel to the trend of the belt.

The N-S Eocene collision resulted in crustal shortening accommodated by thrusts and nappes and incipient crustal subduction. Considering that this collision involved an extremely thinned lithosphere, the N-S closure of this domain may have resulted in E-W flow of the asthenospheric mantle beneath the North Pyrenean Zone but also in a high-temperature deformation of the two lithospheric walls (Figure 6c). A similar process of lateral mantle flow has been previously proposed by *Russo and Silver* [1994] to explain splitting measurements in western South America. In the Pyrenees, such deformation should result in E-W preferred orientation of olivine *a* axis, similar to the fabrics expected during the previous strike-slip episode. We note that the lateral anisotropy variations along the North Pyrenean Zone are consistent with the hypothesis of material extrusion in front of the

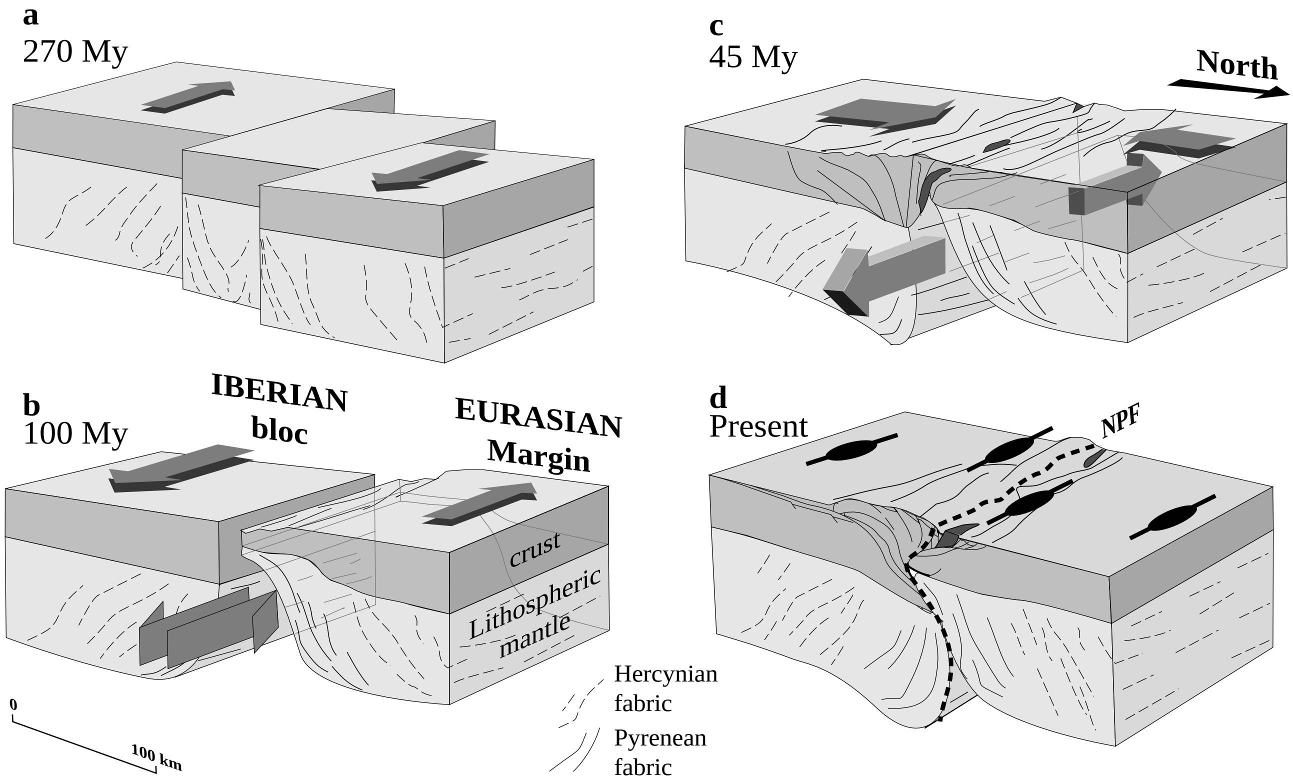

Figure 6. Schematic lithospheric-scale blocs diagrams illustrating the evolution of the Pyrenees since late Hercynian times. (a) At the end of the Variscan orogeny (270 Ma), a large-scale dextral strike-slip fault occurs at the future place of the Pyrenean belt, generating a strong pervasive deformation of the upper mantle. (b) During Albian times (about 100 Ma), the rotation of the Iberian bloc with respect to the Eurasian plate, induced by the North Atlantic and the bay of Biscaye opening, created a long and narrow rift on a sinistral transcurrent zone (the present-day North Pyrenean Zone). This episode is accompanied by asthenospheric upwelling, lherzolite emplacement at very shallow depth, and high-temperature metamorphism of the rift sediments. We propose that both the asthenospheric wedge beneath the rift and the neighboring lithospheres may be pervasively deformed at that stage, with an E-W trending lineation. (c) As proposed by *Mattauer* [1990], at upper Cretaceous (around 80 Ma) the N-S motion of the Iberian bloc began, inducing the closure of the E-W trending rift. We suggest that the hot upper mantle between the two lithospheric blocs may have been laterally extruded. E-W trending lineations could results from this deformation in both the asthenosphere and deep lithosphere. (d) The present-day upper mantle structures beneath the belt could correspond to steeply dipping foliations and E-W trending lineations, acquired either during the Pyrenean built-up (since 100 Ma) for the central part of the belt or during the late Hercynian tectonic episodes for the external parts of the belt. Part of the observed anisotropy may result from present-day upper mantle flow related to the convergence between the two lithospheres. The Hercynian upper mantle pervasive deformation is schematized by dashed lines and the Pyrenean (active or frozen) fabric by continuous lines.

northward moving Iberian plate; δt is much smaller in the central part of the belt (LTE, MLS, BDB) than on the eastern (MTH and BSD) and western edges (PYO and RVH), where the mantle flow is expected to be maximum. That may represent a stagnation point where the strain is expected to be small or null [*Russo and Silver*, 1994].

The closure and the cooling of the system likely resulted at present day in a complex upper mantle structure beneath the central part of the belt, derived from high-temperature mantle deformation, either in the deep lithosphere or in the asthenosphere trapped between the two lithospheric blocs during collision (Figure 6d). Part of this hot mantle may have been incorporated into the lithosphere by cooling and part may remain beneath the NPZ. Although the present-day deformation of the Pyrenees is small, it may be accommodated by upper mantle flow. Therefore part of the recorded anisotropy may be related to active upper mantle deformation beneath the belt. Since the deformation regime of the Pyrenees did not change significantly since Eocene times, a possible anisotropy generated by present-day mantle flow beneath the Pyrenees cannot be distinguished from the previously developed fabric.

In summary, stations located in the Pyrenean Axial Zone (TRG, VIH, PON, LAR, and AUS) and in the North Pyrenean Zone (BSD, MLS, BDB, PYO, and RVH) may therefore likely record a "true" Pyrenean anisotropy, that is, an anisotropy related to either frozen or active Pyrenean tectonics.

5.4. Hercynian Anisotropy

Farther south (at GRF, AVL, RON, for instance), it is unlikely that the Pyrenean orogeny reactivated the whole upper mantle fabric (see discussion of *Vauchez and Barruol* [1996]). A pre-Pyrenean origin of anisotropy is likely for these stations. As suggested by *Arthaud and Matte* [1977] and more recently by *Gleizes et al*. [1997], the whole Pyrenean belt was involved in a broad zone of dextral strike slip motion during the late stage of the Variscan orogen (Figure 6a). Field observations reveal the presence of an E-W trending zone of transpression, characterized by steeply dipping foliations, particularly in the eastern and central Pyrenees [*Carreras and Cirès*, 1986; *Soliva*, 1992]. Such a strike-slip regime of deformation is particularly efficient at generating large magnitude of anisotropy; first, because it may coherently deform the whole lithosphere and, second, because it creates steeply dipping foliations and horizontal lineations, a structural fabric that appears as the most anisotropic for a vertically propagating shear wave, both in the crust [*Barruol and Mainprice*, 1993] and in the upper mantle [*Mainprice and Silver*, 1993].

At FRS in the southern Massif Central, although ϕ is roughly parallel to the Eurasian plate motion vector, it is also consistent with the Hercynian fabric. The axial zone of the "Montagne Noire" (see Figure 1) is composed of a gneissic dome elongated N070°E, parallel to a late Hercynian dextral strike slip fault [*Bard*, 1997; *Nicolas et al*., 1977]. The observed fast direction is parallel to the trend of the Hercynian crustal structure and may be compatible with frozen lithospheric deformation. However, the complex pattern of nulls obtained at this site suggests the presence of a complex structure beneath this site, such as dipping symmetry axis of anisotropy or several anisotropic layers. The asthenospheric mantle plume imaged by seismic tomography beneath the Massif Central [*Granet et al*., 1995] can provide such an explanation.

Whether the anisotropy recorded in the Pyrenean Axial Zone (stations VIH and PON in the central Pyrenees, TRG in the eastern Pyrenees, and perhaps ORG, VIL, BRU, and ALB which are very close to its southern boundary; stations NE10, LAR, and RON in the western Pyrenees) is produced by Pyrenean or Hercynian frozen structures remain uncertain. These stations are close to the North Pyrenean Zone, and therefore their anisotropy may reflect the Pyrenean orogeny. The low-velocity strip beneath the Pyrenean Axial Zone (Figure 5a) suggests the presence of low velocity material down to 50-100 km depth. If this low-velocity corresponds to crustal material, part of the total splitting at these stations may reflect deep crustal Pyrenean deformation. On the other hand, if this low-velocity zone corresponds to partial melting, as suggested by *Pous et al*. [1995], part of the splitting may reflect the orientation of the melt films or pockets at depth. However, since the two deformations (Hercynian and Pyrenean) are expected to give similar anisotropy signatures, both effects may be present and cannot be distinguished by shear wave splitting analysis.

6. Conclusions

The three profiles along which teleseismic shear wave splitting is measured give a rather comprehensive view of upper mantle seismic anisotropy beneath the Pyrenean belt. At this scale, seismic anisotropy appears very homogeneous from both the fast split wave polarization direction (N100° to N110°E) and the amplitude of the observed delay times δt (generally above 1 s and often in the range 1.3 to 1.5 s). This clearly points out the existence of a rather large intrinsic anisotropy in the upper mantle.

From (1) the poor correlation of the observed anisotropy with the present-day plate motion, (2) the short-scale variation of the splitting parameters, (3) the parallelism of the fast wave polarization direction with the outcropping crustal structures, and (4) the good fit between the *SKS* anisotropy and the *Pn* anisotropy, we suggest that most of the anisotropy is located within the uppermost mantle, either frozen in the lithosphere or related to present-day upper mantle deformation beneath the central part of the belt. These structures may be related either to the Pyrenean or to the Hercynian orogeny.

We suggest that the stations located outside and on the external units of the belt record an anisotropy due to a regional-scale transcurrent Hercynian deformation. On the other hand, stations located on the North Pyrenean Zone and perhaps on the Axial Zone of the Pyrenees, the two units most affected by the Pyrenean tectonics, are compatible with upper mantle deformation due to the Pyrenean orogeny. The first episode of this orogeny is a sinistral strike-slip motion of Iberia relative to Eurasia that occurred during Albian times, 100 Ma, and generated elongated rift zones, associated with asthenospheric mantle upwelling. The second episode that may have affected the upper mantle structure is the N-S collision between the two plates that took place mainly during Eocene times, about 45 Ma. We propose that lateral mantle extrusion during the N-S closure of the rift may explain the large E-W anisotropy observed along the belt. Since the convergence regime did not change significantly since Eocene times, part of the anisotropy recorded in the central part of the belt may reflect an active upper mantle flow related to present-day tectonics.

No particularly large variation in anisotropy is correlated with the North Pyrenean Fault. This fault represents the former boundary between the Iberian and the Eurasian plates, along which the relative plate motions could have induced a local increase of deformation and anisotropy. This is not the case: The deformation along this fault is either too narrow at depth to be visible by the technique we use, or it is not stronger than the neighboring pervasive Pyrenean deformation.

Acknowledgments. This project is a contribution to the program Imagerie et Dynamique de la Lithosphère (IDYL) supported by the CNRS/INSU. Many thanks to all the people that helped us during the field surveys, particularly R. Russo, W. Ben Ismail, A. Tommasi, E. Ferreira, F. Samarcq, M. Sylvander, M. Vadell, A Rigo, J.M. Douchain, and also to J. F. Fels for his help in data processing. We are grateful to P. Silver for allowing us to use his splitting analysis program. We also thanks the mayors and farmers of several villages for their help in providing site installations, in particular, at La Salvetat sur Agout, Bessède de Sault, Aussurucq, and Ramous-Puyoo. We are also indebted to the Catalan Seismic Survey which allowed us to set up some stations on their sites. J.T. and J.C. acknowledge support from project UPV001.310-EB003/95. The comments and suggestions of K. Fischer, J. Ni, and R. Russo contributed significantly to the final version of this paper.

References

Arthaud, F., and P. Matte, Late Paleozoic strike-slip faulting in southern Europe and northern Africa: Result of a right-lateral shear zone between the Appalachians and the Urals, *Geol. Soc. Am. Bull.*, *88*, 1305-1320, 1977.

Banda, E., and P. Santanach, The Valencia trough (western Mediterranean): An overview, *Tectonophysics*, *208*, 183-202, 1992.

Bard, J.P., Démembrement anté-Mésozoïque de la chaîne varisque d'Europe occidentale et d'Afrique du Nord: Rôle essentiel des grands décrochements transpressifs dextres accompagnant la rotation-translation horaire de l'Afrique durant le Stéphanien, *C. R. Acad. Sci., Ser. 2*, 324, 693-704, 1997.

Barruol, G., and D. Mainprice, A quantitative evaluation of the contribution of crustal rocks to the shear wave splitting of teleseismic *SKS* waves, *Phys. Earth Planet. Inter*., *78*, 281-300, 1993.

Barruol, G., and A. Souriau, Anisotropy beneath the Pyrenees range from teleseismic shear wave splitting, *Geophys. Res. Lett*., *22*, 493-496, 1995.

Bartrina, M.T., L. Cabrera, M.J. Jurado, J. Guimera, and E. Roca, Evolution of the central Catalan margin of the Valencia trough (western Mediterranean), *Tectonophysics*, *203*, 219-247, 1992.

Ben Ismail, W., and D. Mainprice, An olivine fabric database: An overview of upper mantle fabrics and seismic anisotropy, *Tectonophysics*, in press, 1998.

Bormann, P., G. Gruenthal, R. Kind, and H. Montag, Upper mantle anisotropy underneath central Europe: Effect of absolute plate motion and lithosphere-asthenosphere boundary topography?, *J. Geodyn*., *22*, 11-32, 1996.

Carreras, J., and J. Cirès, The geological significance of the western termination of the Mérens fault at Port Vell (Central Pyrenees), *Tectonophysics*, *129*, 99-114, 1986.

Casas, A., P. Kearey, L. Rivero, and C.R. Adam, Gravity anomaly map of the Pyrenean region and a comparison of the deep geological structure of the western and eastern Pyrenees, *Earth Planet. Sci. Lett*., *150*, 65-78, 1997.

Choukroune, P., Tectonic evolution of the Pyrenees, *Annu. Rev. Earth Planet. Sci*., *20*, 143-158, 1992.

Crampin, S., Effective anisotropic elastic constants for wave propagation through cracked solids, *Geophys. J. R. Astron. Soc*., *76*, 135-145, 1984.

Daignières, M., J. Gallart, E. Banda, and A. Hirn, Implication of the seismic structure for the orogenic evolution of the Pyrenees range, *Earth Planet. Sci. Lett*., *57*, 88-110, 1982.

De Cabissole, B., Apport des données gravimétriques à la connaissance de la chaîne des Pyrénées le long du profil ECORS, doctorat thesis, Univ. de Montpellier II, Montpellier, France, 1989.

Delouis, B., H. Haessler, A. Cisternas, and L. Rivera, Stress tensor determination in France and neighbouring regions, *Tectonophysics*, *221*, 413-437, 1993.

DeMets, C., R.G. Gordon, D.F. Argus, and S. Stein, Current plate motions, *Geophys. J. Int*., *101*, 425-478, 1990.

Gallart, J., N. Vidal, J.J. Danobeitia, and ESCI Group, Lateral variations in the deep structure at the Iberian margin of the Valencia trough imaged from seismic reflection methods, *Tectonophysics*, *232*, 59-75, 1994.

Gleizes, G., D. Leblanc, and J.L. Bouchez, Variscan granites of the Pyrenees revisited: Their role as syntectonic markers of the orogen, *Terra Nova*, *9*, 38-41, 1997.

Golberg, J.M., and A.F. Leyreloup, High temperature-low pressure Cretaceous metamorphism related to crustal thinning (eastern North Pyrenean Zone, France), *Contrib. Mineral. Petrol*., *104*, 194-207, 1990.

Grandjean, G., Mise en évidence des structures crustales dans une partion de chaîne et de leur relation avec les bassins sédimentaires. Application aux Pyrénées occidentales au travers du projet ECORS Arzacq-Pyrénées, doctorat thesis, Univ. de Montpellier II, Montpellier, France, 1992.

Grandjean, G., Etude des structures crustales dans une portion de chaîne et de leur relation avec les bassins sédimentaires. Application aux Pyrénées occidentales, *Bull. Cent. Rech. Explor. Prod. Elf Aquitaine*, *18*, 391-420, 1994.

Granet, M., G. Stoll, J. Dorel, U. Achauer, G. Poupinet, and K. Fuchs, Massif Central (France): New constraints on the geodynamical evolution from teleseismic tomography, *Geophys. J. Int*., *121*, 33-48, 1995.

Granet, M., U. Achauer, and S. Judenherc, Using anisotropic Pn tomography and SKS-wave splitting analysis to investigate the geotectonic setting of upper mantle structures beneath France, *Terra Nova* , *9*, p. 75, EUG, Strasbourg, France, 1997.

Gripp, A.E., and R.G. Gordon, Current plate velocities relative to the hotspots incorporating the Nuvel-1 global plate motion model, *Geophys. Res. Lett*., *17*, 1109-1112, 1990.

Herquel, G., G. Wittlinger, and J. Guilbert, Anisotropy and crustal thickness of northern Tibet: New constraints for tectonic models, *Geophys. Res. Lett*., *22*, 1925-1928, 1995.

Ji, S., X. Zhao, and D. Francis, Calibration of shear-wave splitting in the subcontinental upper mantle beneath active orogenic belts using ultramafic xenoliths from the Canadian cordillera and Alaska, *Tectonophysics*, *239*, 1-27, 1994.

Kennett, B.L.N., Seismic traveltime tables, in *Global Earth Physics: A Handbook of Physical Constants*, AGU Ref. Shelf, vol 1, edited by T.J. Ahrens, pp. 126-143, AGU, Washington, D. C., 1995.

Mainprice, D., and P.G. Silver, Interpretation of *SKS*-waves using samples from the subcontinental lithosphere, *Phys. Earth Planet. Inter*., *78*, 257-280, 1993.

Marson-Pidgeon, M., and M.K. Savage, Frequency-dependent anisotropy in Wellington, New Zealand, *Geophys. Res. Lett*., *24*, 3297-3300, 1997.

Mattauer, M., Une autre interprétation du profil ECORS Pyrénées, *Bull. Soc. Géol. Fr*., *VI*, (8), 307-311, 1990.

McNamara, D.E., and T.J. Owens, Azimuthal shear wave velocity anisotropy in the Basin and Range province using Moho *Ps* converted phases, *J. Geophys. Res*., *98*, 12003-12017, 1993.

Nicolas, A., and N.I. Christensen, Formation of anisotropy in upper mantle peridotites-A review, in *Composition, Structure and Dynamics of the Lithosphere-Asthenosphere System*, Geodyn. Ser., vol. 16, edited by K. Fuchs, and C. Froidevaux, pp. 111-123, AGU, Washington, D.C., 1987.

Nicolas, A., J.L. Bouchez, J. Blaise, and J.P. Poirier, Geological aspects of deformation in continental shear zones., *Tectonophysics*, *42*, 55-73, 1977.

Olivet, J.L., Kinematics of the Iberian plate, *Bull. Cent. Rech. Explor. Prod Elf Aquitaine*, *20*, 131-195, 1996.

Poupinet, G., A. Souriau, M. Vadell, and J.D. Njike-Kassala, Constraints on the lithospheric structure beneath the North Pyrenean Fault from teleseismic observations, *Geology*, *20*, 157-160, 1992.

Pous, J., J. Ledo, A. Marcuello, and M. Daignières, Electrical resistivity model of the crust and upper mantle from magnetotelluric survey through the central Pyrenees, *Geophys. J. Int*., *121*, 750-762, 1995.

Rebai, S., H. Philip, and A. Taboada, Modern tectonic stress field in the Mediterranean region: Evidence for variation in stress directions at different scales, *Geophys. J. Int*., *110*, 106-140, 1992.

Rigo, A., H. Pauchet, A. Souriau, A. Grésillaud, M. Nicolas, C. Olivera, and S. Figueras, The February 1996 earthquake sequence in the eastern Pyrenees: First results, *J. Seismol*., *1*, 3-14, 1997.

Roure, F., and ECORS Pyrenees Team, ECORS deep seismic data and balanced cross sections: Geometric constraints on the evolution of the Pyrenees, *Tectonics*, *8*, 23-39, 1989.

Russo, R.M., and P.G. Silver, Trench-parallel flow benath the Nazca plate from seismic anisotropy, *Science*, *263*, 1105-1111, 1994.

Savage, M., and P. Silver, Mantle deformation and tectonics: Constraints from seismic anisotropy in western United States, *Phys. Earth Planet.*

Inter., *78*, 207-227, 1993.
Séguret, M., and M. Daignières, Crustal scale balanced cross-sections of the Pyrenees; discussion, *Tectonophysics, 129*, 303-318, 1986.
Silver, P.G., Seismic anisotropy beneath the continents: Probing the depths of the geology, *Annu. Rev. Earth Planet. Sci*., *24*, 385-432, 1996.
Silver, P.G., and W.W. Chan, Shear wave splitting and subcontinental mantle deformation, *J. Geophys. Res*., *96*, 16429-16454, 1991.
Silver, P.G., and M.K. Savage, The interpretation of shear-wave splitting parameters in the presence of two anisotropic layers, *Geophys. J. Int*., *119*, 949-963, 1994.
Soliva, J., Les déformations ductiles dans la zone axiale des Pyrénées orientales, doctorat thesis, Univ. de Montpellier II, Montpellier, France, 1992.
Souriau, A., and M. Granet, A tomographic study of the lithosphere beneath the Pyrenees, from local and teleseismic data, *J. Geophys. Res*., *100*, 18117-18134, 1995.
Souriau, A., and J.D. Njike-Kassala, Anisotropy beneath the North Pyrenean Fault, *Phys. Earth Planet. Inter*., *78*, 239-244, 1993.
Tommasi, A., A. Vauchez, and R. Russo, Seismic anisotropy in oceanic basins: Resistive drag of the sublithospheric mantle?, *Geophys. Res. Lett*., *23*, 2991-2994, 1996.
Torne, M., B. De Cabissole, R. Bayer, A. Casas, M. Daignières, and A. Rivero, Gravity constraints on the deep structures of the Pyrenean belt along the ECORS profile, *Tectonophysics*, *166*, 105-116, 1989.
Vauchez, A., and G. Barruol, Shear wave splitting in the Appalachians and the Pyrenees: Importance of the inherited tectonic fabric of the lithosphere, *Phys. Earth Planet. Inter*., *95*, 127-138, 1996.
Vegas, R., The Valencia trough and the origin of the western Mediterranean basins, *Tectonophysics*, *203*, 249-261, 1992.
Vielzeuf, D., and J. Kornprobst, Crustal splitting and the emplacement of the Pyrenean lherzolites and granulites, *Earth Planet. Sci. Lett*., *67*, 87-96, 1984.
Vinnik, L.P., L.I. Makeyeva, A. Milev, and A.Y. Usenko, Global patterns of azimuthal anisotropy and deformations in the continental mantle, *Geophys. J. Int*., *111*, 433-437, 1992.
Zoback, M.L., First- and second-order patterns of stress in the lithosphere: The World Stress Map Project, *J. Geophys. Res*., *97*, 11703-11728, 1992..

G. Barruol and A. Vauchez, Laboratoire de Tectonophysique, CNRS, Université Montpellier II, 34095 Montpellier cedex 5, France. (Email: barruol@dstu.univ-montp2.fr; vauchez@dstu.univ-montp2.fr)

A. Souriau, Laboratoire de Dynamique Terrestre et Planétaire, CNRS, 14 av Belin, 31055 Toulouse, France. (Email: souriau@pontos.cst.cnes.fr)

J. Diaz and J. Gallart, Institut de Ciències de la Terra "Jaume Almera", CSIC, c/ Lluis Sole Sabaris, E-08028 Barcelona, Spain. (Email: jdiaz@ija.csic.es; jgallart@ija.csic.es)

J. Tubia and J. Cuevas, Departamento de Geodinamica, Universidad del Pais Vasco, Apartado 644 48080 Bilbao, Spain.

(Received November 25, 1997; revised May 22, 1998;
accepted August 14, 1998.)